Cellular/Molecular

$P2Y_6$ Receptor-Dependent Microglial Phagocytosis of Synapses during Development Regulates Synapse Density and Memory

Jacob M. Dundee,[1] Mar Puigdellívol,[1,2] Richard Butler,[3] and Guy C. Brown[1]

[1]Department of Biochemistry, University of Cambridge, Cambridge, CB2 1QW, United Kingdom, [2]Institute of Neurosciences, University of Barcelona, Barcelona, 08035, Spain, and [3]The Wellcome Trust Cancer Research UK Gurdon Institute, University of Cambridge, Cambridge, CB2 1QN, United Kingdom

During brain development, excess synapses are pruned (i.e., removed), in part by microglial phagocytosis, and dysregulated synaptic pruning can lead to behavioral deficits. The $P2Y_6$ receptor ($P2Y_6R$) is known to regulate microglial phagocytosis of neurons, and to regulate microglial phagocytosis of synapses in cell culture and *in vivo* during aging. However, currently it is unknown whether $P2Y_6R$ regulates synaptic pruning during development. Here, we show that $P2Y_6R$ KO mice of both sexes had strongly reduced microglial internalization of synaptic material, measured as Vglut1 within CD68-staining lysosomes of microglia at postnatal day 30 (P30), suggesting reduced microglial phagocytosis of synapses. Consistent with this, we found an increased density of synapses in the somatosensory cortex and the CA3 region and dentate gyrus of the hippocampus at P30. We also show that adult $P2Y_6R$ KO mice have impaired short- and long-term spatial memory and impaired short- and long-term recognition memory compared with WT mice, as measured by novel location recognition, novel object recognition, and Y-maze memory tests. Overall, this indicates that $P2Y_6R$ regulates microglial phagocytosis of synapses during development, and this contributes to memory capacity.

Key words: **developmental biology; memory; microglia; $P2Y_6$ receptor; phagocytosis; synaptic pruning**

Significance Statement

The $P2Y_6$ receptor ($P2Y_6R$) is activated by uridine diphosphate released by neurons, inducing microglial phagocytosis of such neurons or synapses. We tested whether $P2Y_6R$ regulates developmental synaptic pruning in mice and found that $P2Y_6R$ KO mice have reduced synaptic material within microglial lysosomes, and increased synaptic density in the brains of postnatal day 30 mice, consistent with reduced synaptic pruning during development. We also found that adult $P2Y_6R$ KO mice had reduced memory, consistent with persistent deficits in brain function, resulting from impaired synaptic pruning. Overall, the results suggest that $P2Y_6R$ mediates microglial phagocytosis of synapses during development, and the absence of this results in memory deficits in the adult.

Introduction

During development, synapse formation in the human brain is thought to peak at 1 million synapses per second (Tang et al., 2001). Excess synapses are generated compared with what remains in adulthood, and some of these synapses are then pruned to shape neuronal networks in an activity-dependent manner (Hong et al., 2016b; Faust et al., 2021). This synaptic pruning is by multiple mechanisms but is partly mediated by microglial phagocytosis of the synapses (Stevens et al., 2007; Tremblay et al., 2010; Paolicelli et al., 2011; Schafer et al., 2012; Mordelt and de Witte, 2023).

Microglia are CNS-resident macrophages that play a variety of roles in maintaining a healthy brain. One such role involves the phagocytosis (i.e., engulfment and degradation) of synapses, neurons, debris, bacteria, and aggregated proteins (Sierra et al., 2013; Wolf et al., 2017; Tay et al., 2018; Gabandé-Rodríguez et al., 2020). Microglial phagocytosis of synapses is involved in learning and memory in adults (Miyanishi et al., 2021), but excessive microglial phagocytosis of the synapses may contribute to memory loss with aging and neurodegeneration (Hong et al., 2016a; Dundee et al., 2023). Signals regulating microglial phagocytosis of synapses include fractalkine and the fractalkine

Received May 15, 2023; revised July 27, 2023; accepted Aug. 31, 2023.

Author contributions: J.M.D. and M.P. performed research; J.M.D., M.P., and R.B. analyzed data; J.M.D. and G.C.B. wrote the first draft of the paper; J.M.D. and G.C.B. edited the paper; J.M.D. and G.C.B. wrote the paper; G.C.B. designed research.

This work was supported by Medical Research Council UK MR/L010593; Biotechnology and Biological Sciences Research Council BB/T508160/1; and Eli Lilly ARUK-DC2017-4 and RG99704. We thank Bernard Robaye for the $P2Y_6R$ KO mice; Stefan Milde for carrying out the behavioral tests on 9- to 12-month-old mice; and the Cambridge Advanced Imaging Center for support and assistance in this work.

The authors declare no competing financial interests.

Correspondence should be addressed to Guy C. Brown at gcb3@cam.ac.uk.

https://doi.org/10.1523/JNEUROSCI.1089-23.2023

receptor, complement components C1q, C3, and C4, and complement receptor 3, adenosine 2A, TREM2, GPR56, phosphatidylserine, CD47, TGFb, and the $P2Y_6$ receptor ($P2Y_6R$) (Faust et al., 2021; Dundee et al., 2023).

$P2Y_6R$ is a GPCR for extracellular uridine diphosphate (UDP), expressed from the *P2ry6* gene by myeloid and other cells in the body, but in the brain, is almost exclusively expressed by microglia (Koizumi et al., 2007). Koizumi et al. (2007) found that kainite-stressed neurons released uridine triphosphate (UTP), which was hydrolyzed into UDP and induced microglia to phagocytose neurons via activating $P2Y_6R$ on microglia. We subsequently showed that extracellular UDP could induce microglia to phagocytose live neurons, and that inhibition of $P2Y_6R$ prevented neuronal loss induced by LPS in glial-neuronal cultures and in mouse brains *in vivo* (Neher et al., 2014; Milde et al., 2021). $P2Y_6R$ KO also prevented microglial phagocytosis of neurons and loss of neurons and memory induced β amyloid and TAU *in vivo* (Puigdellívol et al., 2021).

Recently, we reported that $P2Y_6R$ regulated microglial phagocytosis of synapses (Dundee et al., 2023). In culture, we showed that $P2Y_6R$ inhibition or KO strongly reduced microglial phagocytosis of isolated synapses (synaptosomes), and that glial-neuronal cultures from $P2Y_6R$ KO mice had reduced inflammatory loss of synapses (Dundee et al., 2023). *In vivo*, we found that $P2Y_6R$ KO prevented an aging-associated increase in microglial phagocytosis of synapses, and reduced loss of synapses and memory with age (Dundee et al., 2023).

Here, we investigated whether $P2Y_6R$ regulated microglial phagocytosis of synapses during development, and whether this affected synaptic density and memory. We found that microglia from $P2Y_6R$ KO mice had reduced internalization of synaptic material at postnatal day 30 compared with WT mice, coupled with an increase in synaptic density in three different regions of $P2Y_6R$ KO mouse brains. $P2Y_6R$ KO mice also performed worse than WT mice in both long- and short-term memory tests. These findings are significant as they support the hypothesis that microglial phagocytosis of synapses during development contributes to a healthy brain and this is, in part, through activation of $P2Y_6R$.

Materials and Methods

Animals. All animal work was conducted in accordance with the Animals (Scientific Procedures) Act 1986 Amendment Regulations 2012 following ethical review by the University of Cambridge Animal Welfare and Ethical Review Body. $P2Y_6R$ KO mice were kindly provided by Bernard Robaye (ULB Brussels) and maintained on a C57BL/6 background (Charles River Laboratories). $P2Y_6R$ KO mice and WT littermates were used to establish homozygous $P2Y_6R$ WT and KO sublines. Postnatal day 30 (P30) mice included 4 male and 4 female WT mice and 4 male and 4 female $P2Y_6R$ KO mice. Four-month-old mice included 6 male and 5 female WT mice and 8 male and 3 female $P2Y_6R$ KO mice. Nine- to 12-month-old mice included 9 female WT mice and 7 female $P2Y_6R$ KO mice. Mice used in short-term memory tests received intracerebroventricular injections of 4 μl PBS 3 or 14 d before testing.

Fixation and tissue sectioning. P30 mice were killed following cervical dislocation and decapitation. Brains were removed and fixed for 48 h in 4% PFA and cryoprotected by immersion in an increased 10%-30% sucrose solution until sectioning. Serial coronal sections (25 μm) through the whole brain were collected using a sliding microtome and placed in PBS with 0.025% sodium azide as free-floating sections.

Immunohistochemistry of free-floating brain slices. All steps were conducted at room temperature, with shaking, and rinsing 3 times with PBS after each incubation unless stated otherwise. Five to six free-floating 25 μm sections were taken every 12th brain section of 8 $P2Y_6R$ WT and KO mice at P30 for immunohistochemistry. Sections were rinsed 3 times in PBS and incubated with 50 mM ammonium chloride in PBS for 30 min to quench free aldehyde groups from fixation. Sections were then incubated in 0.1% Sudan Black B in 70% ethanol for 20 min to reduce autofluorescence, permeabilized using 1% Triton X-100 in PBS for 30 min to facilitate antibody penetration, and blocked for 1 h with blocking solution (2% BSA, 3% goat serum, and 0.03% Triton X-100 in PBS). Subsequently, sections were incubated with mouse anti-Vglut1 (1:200, Fisher Scientific, MA5-31 373), rabbit anti-Homer1 (1:500, Synaptic Systems, 160003), rabbit anti-Iba1 (1:200, Wako, 019-19 741), and rat CD68 (1:200, Fisher Scientific, 14-0681-82) antibodies in blocking solution for 2 h at 37°C (Xiao et al., 2017). Sections were then rinsed 3 times with PBS and then incubated with AlexaFluor-568 goat anti-mouse (1:200, Fisher Scientific, A5054), AlexaFluor-goat 488 anti-rabbit (1:200, Fisher Scientific, A11008), and AlexaFluor-647 goat anti-rat (1:200, Fisher Scientific, A21247) antibodies for 2 h at 37°C. Sections were then rinsed 3 times with PBS and mounted on poly-L-lysine-treated glass slides and dried at 37°C. Sections were then mounted using Vectashield mounting medium with DAPI (Vector Laboratories, H1500) and imaged using confocal microscopy.

Synaptic internalization analysis of free-floating brain sections. Imaging was conducted on a Nikon C2si confocal microscope with a 63×, 1.35 NA oil immersion objective using 488, 561, and 640 nm laser lines. Microglia were imaged and analyzed following Schafer et al. (2014). Briefly, *Z* stacks (0.5 μm step intervals) were collected, being 2 μm from the surface of the section at each ROI. Fourteen to 15 microglia were analyzed across three sections 300 μm apart per mouse. Background subtraction (6 pixels/0.2 μm rolling ball) and intensity normalization (2%) across the sections were conducted using Fiji (Schindelin et al., 2012). Microglial structures were analyzed using 3DMorph analysis (York et al., 2018). Microglial (Iba1), lysosomal (CD68), and synaptic (Vglut1) surface rendering was conducted using Imaris 9.1.2. The results for the surface-rendered objects were represented as volume (μm^3).

Microglial density of free-floating brain sections. Imaging was conducted on an EVOS M5000 fluorescent microscope with a 20× objective. Nine images in the somatosensory cortex were taken across three sections 300 μm apart per mouse. Total microglia (Iba1- and DAPI-positive) per field were counted using Fiji (Schindelin et al., 2012).

Synaptic density analysis of free-floating brain sections. Imaging was conducted on a Nikon C2si confocal microscope with a 63×, 1.35 NA oil immersion objective using 405, 488, and 561 nm laser lines. A 2 μm *Z* stack (0.125 μm step intervals) was collected, being 2-5 μm from the surface of the section at each ROI. Nine images were taken across three sections 300 μm apart per mouse. Background subtraction (6 pixels/0.2 μm rolling ball) and intensity normalization (2%) across the sections were conducted using Fiji (Schindelin et al., 2012). We developed a custom script for Fiji to map Vglut1 and Homer1 puncta positions in 3D and analyze their distributions. In order to detect puncta 0.2 μm in diameter (Moreno Manrique et al., 2021), the script applies a Laplacian of Gaussian filter with the SD set from this estimated diameter and detects local maxima as puncta candidates. Candidate points are then clustered into final puncta by merging points within one punctum width of each other, excluding points on image edges and below the global Otsu intensity threshold (Otsu et al., 1979). The number of puncta "colocalized" between the two channels is counted as the number of C2 (Homer1) coordinates having at least one C3 (Vglut1) coordinate within one punctum width. Local density is calculated for each punctum using a Gaussian kernel density estimate (Davis et al., 1956), and overall density in each channel is calculated as puncta per μm^3. The puncta densities were normalized to the mean of WT mice.

Long-term novel object location test and novel object recognition test. To test long-term location and recognition memory, object location recognition testing (OLRT) and novel object recognition testing (NORT) were performed in a 30 × 44 cm arena with opaque sides, with a 24 h retention time (Murai et al., 2007; Puigdellívol et al., 2021). Briefly, 4-month-old mice were first habituated to the arena in the absence of objects on 2 consecutive days (15 min/day), when spontaneous locomotor activity (total distance traveled) and anxiety/motivation (distance

traveled in periphery vs center of the open field) were measured. On the third day, visual clues were included on the walls of the open field and two similar objects were presented for 10 min (A and A′ objects). Twenty-four hours later, the same animals were retested for 5 min retention test in the arena with a familiar (A) and a new (B) object location. The object location preference was measured as the time exploring each object × 100/time exploring both objects. On the fifth day, visual clues were removed and two new identical objects were presented to the animals for 10 min (C and C′). Twenty-four hours later, the same animals were retested for 5 min retention test in the arena with a familiar (C) and a new (D) object. The object preference was measured as the time exploring each object × 100/time exploring both objects. Animals were tracked and recorded with SMART Junior software (Panlab). Objects and arena were cleaned thoroughly with 70% ethanol and dried after each trial to eliminate odor cues. The experimenter was blinded to the genotype of the individual animals. NORT data were reanalyzed from Dundee et al. (2023).

Short-term novel object recognition memory test. To test short-term recognition memory, NORT was performed in a 30 × 44 cm arena with opaque sides, with a 2 min retention time (Puigdellívol et al., 2021). Briefly, 9- to 12-month-old mice were first habituated to the arena in the absence of objects for two 10 min sessions 2 h apart. The next day, two identical objects were presented for 10 min (A and A′ objects). Two minutes later, the same animals were retested for 5 min in the arena with a familiar (A) and a novel (B) object. The order of testing of mice from different experimental groups was randomized on day 1 and maintained in the same order on day 2. Object interaction times and ratios were extracted from digital recordings of the trials using modified Autotyping software. The experimenter was blinded to the genotype of the individual animals. These data were reanalyzed from Puigdellívol et al. (2021).

Y-maze memory test. To test short-term spatial memory, spontaneous alternation performance in a Y-maze was tested as described previously (Prieur and Jadavji, 2019). Briefly, 9- to 12-month-old mice were placed in the center of the symmetrical Y-maze and were allowed to explore freely through the maze during an 8 min session. The sequence, total number of arms entered, and total distance traveled were recorded. Spontaneous alternations (%) are as follows: number of arm entries that were not identical to the previous arm entry/total number of arm entries × 100. Arm entries and distance traveled were extracted from digital recordings of the trials using modified Autotyping software. The experimenter was blinded to the genotype of the individual animals.

Statistical analysis. Error bars indicate mean ± SEM, and each data point represents 1 animal (see Figs. 1*d-f*, 2*b*,*d*,*e–g*, 3*b*, 4*d*, 5*d*, 6*d*, 7*d*, 8*b–f*, 9*b–d*,*f*,*g*; Extended Data Figs. 4-1*a*, 4-2). Statistical differences were calculated using unpaired *t* tests and one-sample *t* tests. Statistical correlation was conducted using paired Pearson correlation coefficients. All experiments were analyzed using GraphPad Prism 9 (GraphPad Software). Graphical data were shown as individual data points, including mean values with error bars indicating SEM. For each experiment and graph, statistical details including the statistical test used, the exact value of *n*, what *n* represents (number of animals per genotype) as well as dispersion and precision measures (mean, SEM, etc.) can be found in the figure legends.

Code data. All codes used to analyze synaptic puncta can be found at https://github.com/gurdon-institute/Synaptic-Density-Analysis. Experimental data reported in this paper will be shared by the corresponding authors upon request.

Results

$P2Y_6$R KO results in reduced synaptic internalization during development

During development, synaptic levels are regulated in part by the phagocytosis of synapses by microglia (Schafer et al., 2012). We have previously shown that $P2Y_6$R KO microglia have reduced synaptic internalization during aging (Dundee et al., 2023). To test whether $P2Y_6$R is involved in the microglial phagocytosis of synapses during development, we analyzed the internalization of synaptic material within microglial lysosomes in the somatosensory cortex of P30 WT and KO mice by confocal microscopy (Fig. 1*a*). Coronal brain slices were immunostained using antibodies to Iba1 (microglial marker), CD68 (lysosomal marker), and Vglut1 (presynaptic marker), and internalized Vglut1 volume within lysosomal microglia was analyzed by generating *Z*-projection surface renderings using Imaris software (Fig. 1*b*,*c*). We chose a presynaptic marker (Vglut1), rather than a postsynaptic marker, as there is clearer evidence for microglial phagocytosis of presynaptic markers during development (Weinhard et al., 2018; Mordelt and de Witte, 2023). We chose to examine synapse phagocytosis at P30 because synaptic pruning has been reported to still be actively occurring in somatosensory cortex of mice at this time point (Cong et al., 2020). We chose the somatosensory cortex because we have previously found that $P2Y_6$R affects synaptic density in this area during aging (Dundee et al., 2023) and the somatosensory cortex affects working memory (Long and Zhang, 2021).

There was a small but significant increase in microglial Iba1 volume in the $P2Y_6$R KO mice compared with the WT mice (Fig. 1*d*, $n = 7$ or 8, unpaired *t* test, WT: 282, KO: 332, $p = 0.024$, $\eta^2 = 0.269$); however, there were no other observable effects on morphology (York et al., 2018), such as the number of branches ($n = 8$, unpaired *t* test, WT: 63, KO: 60, $p = 0.376$, $\eta^2 = 0.007$), the number of branch points ($n = 8$, unpaired *t* test, WT: 52, KO: 50, $p = 0.391$, $\eta^2 = 0.006$), the average branch length ($n = 8$, unpaired *t* test, WT: 32, KO: 33 $p = 0.327$, $\eta^2 = 0.015$), or the maximum ($n = 8$, unpaired *t* test, WT: 70, KO: 71, $p = 0.393$, $\eta^2 = 0.005$) and minimum ($n = 8$, unpaired *t* test, WT: 4.1, KO: 4.4, $p = 0.178$, $\eta^2 = 0.061$) branch length (Fig. 2). Microglial density was subtly but significantly reduced in $P2Y_6$R KO mice, suggesting a small effect on microglial proliferation at a young age (Fig. 3, $n = 8$, unpaired *t* test, WT: 54, KO: 49, $p = 0.007$, $\eta^2 = 0.357$). There were no significant differences in microglial CD68 volume between WT and KO mice (Fig. 1*e*, $n = 7$ or 8, unpaired *t* test, WT: 4.2, KO: 3.4, $p = 0.210$, $\eta^2 = 0.051$), indicating no difference in microglial lysosomal volume. Virtually all of the CD68 staining was within Iba1-stained microglia (Extended Data Fig. 1-1), indicating that this marker of phagocytic lysosomes was relatively specific to microglia. Importantly, the volume of Vglut1 internalized within microglial CD68 was strongly and significantly lower in the KO mice, indicating that the microglial phagocytosis of synapses is strongly reduced in KO mice (Fig. 1*f*, $n = 7$ or 8, unpaired *t* test, WT: 0.028, KO: 0.007, $p = 0.001$, $\eta^2 = 0.506$). This suggests that $P2Y_6$R mediates the phagocytosis of synapses during development.

$P2Y_6$R KO results in increased synaptic density during development

In order to investigate whether this decrease in microglial phagocytosis of synapses had an effect on synapse density during development, we examined the synaptic density of WT and $P2Y_6$R KO mice at P30. Synaptic density was analyzed in the somatosensory cortex, the hippocampal CA1 and CA3 stratum radiatum, and the dentate gyrus molecular layer of P30 $P2Y_6$R WT and KO mice using confocal microscopy (Figs. 4*a*, 5*a*, 6*a*, 7*a*). Coronal brain slices were immunostained using antibodies to Vglut1 (presynaptic marker) and Homer1 (postsynaptic marker), and synaptic density was measured as colocalized (<200 nm) puncta of both synaptic markers in an entire *Z* stack.

In the somatosensory cortex, the density of Vglut1 puncta ($n = 8$, unpaired *t* test, WT: 100, KO: 105, $p = 0.030$, $\eta^2 = 0.229$)

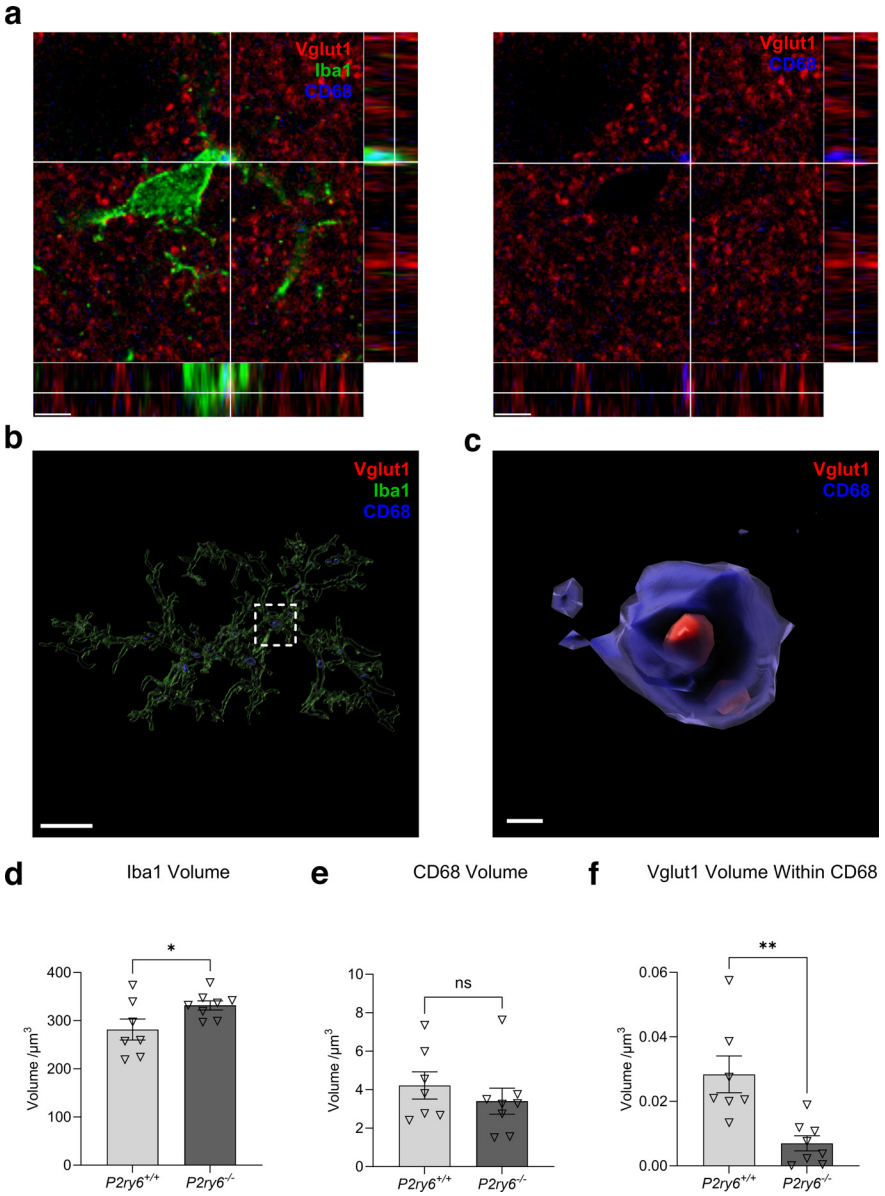

Figure 1. $P2Y_6R$ deficiency reduces synaptic pruning during development. ***a***, Representative confocal microscopy image of mice stained for Iba1 (green, microglial marker), CD68 (blue, lysosomal marker), and Vglut1 (red, synaptic marker) in the somatosensory cortex. Scale bar, 2 μm. Virtually all of the CD68 staining was within Iba1-stained microglia, as shown in Extended Data Figure 1-1. ***b***, Representative surface-rendered microglia (from ***a***). Scale bar, 3 μm. ***c***, Enlarged inset of Vglut1 colocalization within CD68, denoted by the white dotted line (from ***b***). Scale bar, 0.5 μm. Microglial volume (***d***), CD68 volume within microglia (***e***), and Vglut1 colocalization within CD68 (***f***) across P30 WT and $P2Y_6R$ KO mice ($n = 7$ or 8). Each point represents 1 animal comprised of 14-15 microglia analyzed across three equidistant sections. Error bars indicate $\pm$ SEM. ns, $p \geq 0.05$; *$p < 0.05$; **$p < 0.01$; (unpaired *t* test).

and the colocalization of Vglut1 and Homer1 puncta ($n = 8$, unpaired *t* test, WT: 100, KO: 109, $p = 0.039$, $\eta^2 = 0.206$) were significantly increased in KO mice compared with WT mice, with no difference in Homer1 puncta density (Fig. 4*b–d*, $n = 8$, unpaired *t* test, WT: 100, KO: 101, $p = 0.418$, $\eta^2 = 0.003$). No difference in density was observed in the hippocampal CA1 stratum radiatum for Vglut1 puncta ($n = 8$, unpaired *t* test, WT: 100, KO: 98, $p = 0.335$, $\eta^2 = 0.013$), Homer1 puncta ($n = 8$, unpaired *t* test, WT: 100, KO: 102, $p = 0.215$, $\eta^2 = 0.045$), or the colocalization of Vglut1 and Homer1 puncta (Fig. 5*b–d*, $n = 8$, unpaired *t* test, WT: 100, KO: 101, $p = 0.394$, $\eta^2 = 0.005$). In the hippocampal CA3 stratum radiatum, the density of Vglut1 puncta ($n = 8$, unpaired *t* test, WT: 100, KO: 108, $p = 0.038$, $\eta^2 = 0.208$) and the colocalization of Vglut1 and Homer1 puncta ($n = 8$, unpaired *t* test, WT: 100, KO: 115, $p = 0.048$, $\eta^2 = 0.184$) were significantly increased in KO mice compared with WT mice, with no difference in Homer1 puncta (Fig. 6*b–d*, $n = 8$, unpaired *t* test, WT: 100, KO: 108, $p = 0.092$, $\eta^2 = 0.123$). In the molecular layer of the dentate gyrus, the density of Homer1 puncta ($n = 8$, unpaired *t* test, WT: 100, KO: 114, $p = 0.005$, $\eta^2 = 0.388$) and the colocalization of Vglut1 and Homer1 puncta ($n = 8$, unpaired *t* test, WT: 100, KO: 113, $p = 0.027$, $\eta^2 = 0.241$) were significantly increased in KO mice compared with WT mice, with no difference in Vglut1 puncta (Fig. 7*b–d*, $n = 8$, unpaired *t* test, WT: 100, KO: 100, $p = 0.485$, $\eta^2 = 0.0001$). We did not examine synapse density in any other areas of the brain. Raw values for the Vglut1 puncta density, Homer1 puncta density, and the colocalization density are visible in Extended Data Figure 4-1. Furthermore, the Pearson correlation coefficient was calculated comparing the internalization of synaptic material per mouse in the somatosensory cortex

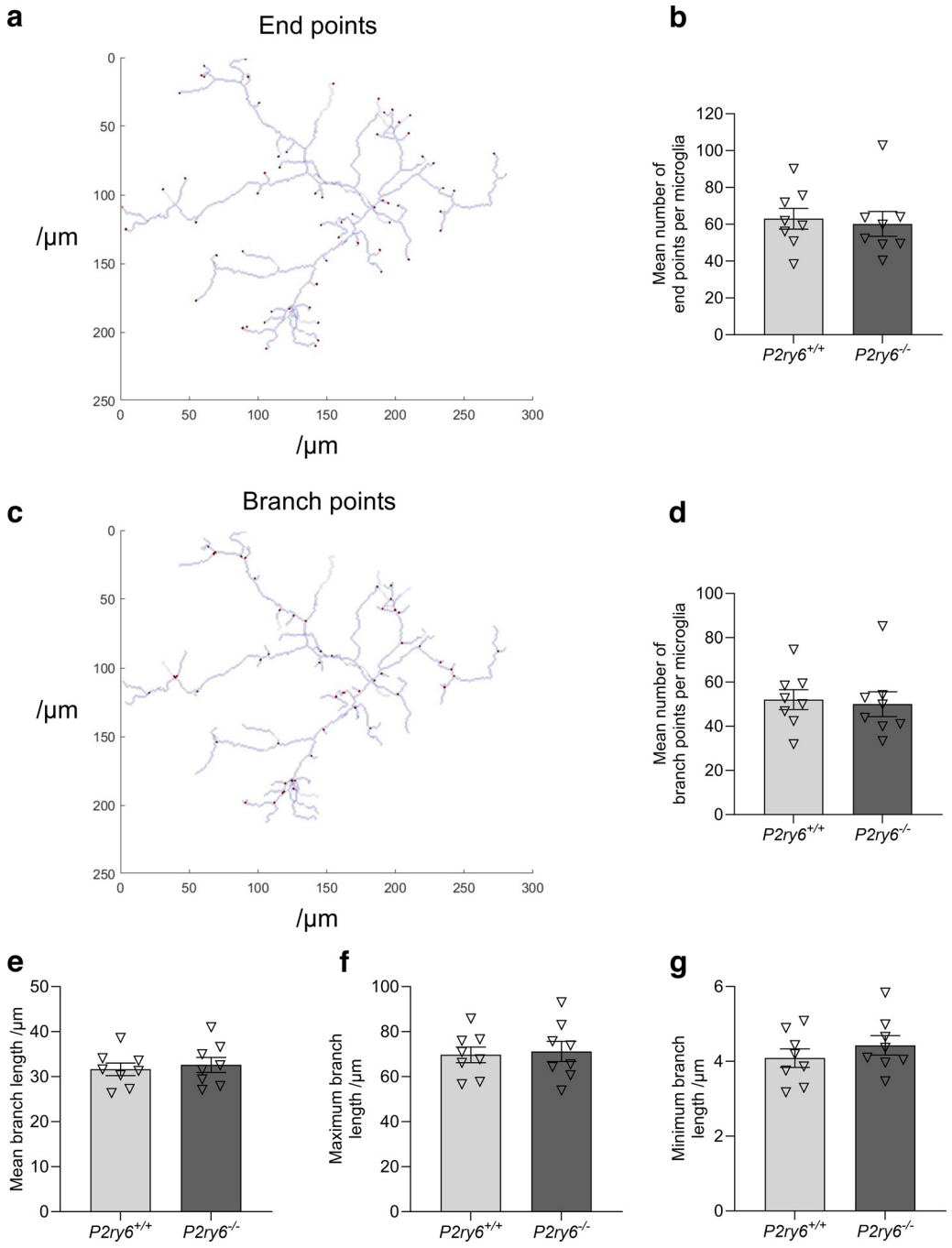

Figure 2. P2Y$_6$R deficiency does not affect microglial branching in the somatosensory cortex at P30. ***a***, Microglial branch end points identified by 3DMorph analysis (York et al., 2018). ***b***, Mean number of branch end points per microglia ($n = 8$). ***c***, Microglial branching points identified by 3DMorph analysis (York et al., 2018). ***d***, Mean number of branching points per microglia ($n = 8$). ***e***, Mean branch length (μm) per microglia ($n = 8$). ***f***, Mean of the maximum branch length (μm) per microglia ($n = 8$). ***g***, Mean of the minimum branch length (μm) per microglia ($n = 8$). Each point represents 1 animal. Statistical comparisons were made via unpaired *t* tests. Error bars indicate ± SEM.

to their corresponding synaptic density. We found a significant, negative correlation between the volume of internalized synaptic material by microglia and the synaptic density in the somatosensory cortex (Extended Data Fig. 4-2, $n = 15$, Pearson correlation coefficient, $r = -0.532$, $p = 0.021$). Together, these data indicate that P2Y$_6$R KO increases synapse density and decreases microglial phagocytosis of synapses during development, and the data are consistent with P2Y$_6$R-mediated microglial phagocytosis of synapses causing synaptic pruning during development.

P2Y$_6$R KO results in reduced memory

In the previous section, we found that P2Y$_6$R KO increased synapse density in the somatosensory cortex and hippocampus, regions that are associated with various forms of memory (Rebola et al., 2017; Hainmueller and Bartos, 2020; Long and Zhang, 2021). Dysregulated synaptic pruning during development has been associated with memory deficits (Wang et al., 2022). And we have previously observed a role for P2Y$_6$R-dependent memory loss in aging, and both an acute amyloid model and chronic tau model of neurodegeneration (Puigdellívol et al., 2021; Dundee et al., 2023).

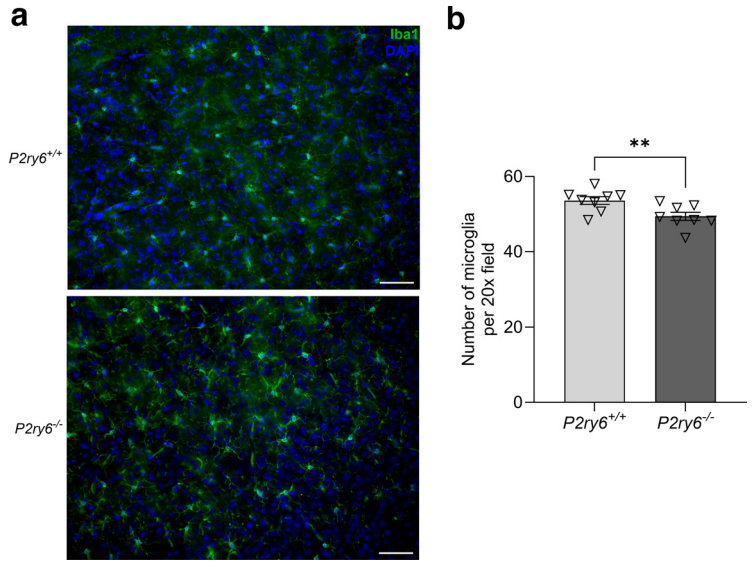

Figure 3. $P2Y_6R$ deficiency reduces microglial density in the somatosensory cortex at P30. ***a***, Representative fluorescent microscopy images of mice stained for Iba1 (green, microglial marker) and DAPI (blue, nuclei marker) in the somatosensory cortex. Scale bar, 50 μm. ***b***, Mean number of microglia per 20× field ($n = 8$). Each point represents 1 animal. Error bars indicate ± SEM. $^{**}p < 0.01$ (unpaired *t* test).

To investigate whether the reduced synaptic pruning in $P2Y_6R$ KO mice had a long-term effect on memory, we tested the memory of adult WT and $P2Y_6R$ KO mice using the OLRT, the NORT, and the Y-maze. The NORT tests object recognition memory (Ennaceur and Delacour, 1988) while the OLRT and Y-maze test spatial memory (Vogel-Ciernia and Wood, 2014; Kraeuter et al., 2019). We first tested long-term spatial memory using the OLRT. Four-month-old mice were habituated in an open field for 2 consecutive days; and on the third day, mice were allowed to explore two identical objects for 10 min in the presence of visual clues on the walls of the open field. Twenty-four hours after this training, one of the objects remained in the same location (familiar) while the other was moved (novel), and the relative time spent with novel and familiar objects was quantified (Fig. 8*a*). During the training session, WT mice had no overall preference for the objects at either location ($n = 11$, one-sample *t* test to 50%, WT: 52, $p = 0.356$, $\eta^2 = 0.086$), while $P2Y_6R$ KO mice had a slight object preference (Fig. 8*b*, $n = 11$, one-sample *t* test to 50%, KO: 54, $p = 0.015$, $\eta^2 = 0.459$). Twenty-four hours after training, WT mice spent more time with the object at the novel location, meaning that they had long-term memory of the object locations (Fig. 8*c*, $n = 11$, one-sample *t* test to 50%, WT: 72, $p = 0.005$, $\eta^2 = 0.556$). However, $P2Y_6R$ KO mice did not show a preference for either object location ($n = 11$, one-sample *t* test to 50%, KO: 55, $p = 0.305$, $\eta^2 = 0.105$) and showed reduced preference compared with WT mice ($n = 11$, unpaired *t* test, WT: 72, KO: 55, $p = 0.023$, $\eta^2 = 0.186$), indicating that KO mice have impaired long-term spatial memory.

Using the same animals, we then tested long-term recognition memory using the NORT. The animals had previously been habituated in the open field (day 1 and 2) followed by the OLT (day 3 and 4). Visual clues were removed from the walls of the open field; and on the fifth day, mice were allowed to explore two new identical objects for 10 min. Twenty-four hours after training, one of the objects (familiar) was replaced by a new object (novel), and the relative time spent with novel and familiar objects was quantified (Fig. 8*d*). During the training session, both WT ($n = 11$, one-sample *t* test to 50%, WT: 56, $p = 0.033$, $\eta^2 = 0.379$) and $P2Y_6R$ KO ($n = 11$, one-sample *t* test to 50%, KO: 55, $p = 0.049$, $\eta^2 = 0.335$) mice had a slight preference for one object (Fig. 8*e*). During the test, both WT ($n = 11$, one-sample *t* test to 50%, WT: 74, $p = 0.0002$, $\eta^2 = 0.770$) and $P2Y_6R$ KO ($n = 11$, one-sample *t* test to 50%, KO: 64, $p = 0.005$, $\eta^2 = 0.564$) mice spent noticeably more time with the novel object, meaning that they had long-term memory of the familiar object. However, $P2Y_6R$ KO mice showed a significantly reduced preference for the novel object compared with WT mice (Fig. 8*f*, $n = 11$, unpaired *t* test, WT: 74, KO: 64, $p = 0.042$, $\eta^2 = 0.142$), indicating that KO mice have impaired long-term recognition memory. These data suggest that long-term memory is impaired in $P2Y_6R$ KO mice.

We tested short-term spatial memory of 9- to 12-month old mice using the Y-maze, where mice were placed in the center of the symmetrical Y-maze and were allowed to explore freely for 8 min (Fig. 9*a*). The sequence, total number of arms entered, and distance traveled were recorded to determine the spontaneous alterations, which is a measure of short-term spatial memory. There was a nonsignificant increase in the number of total arm entries (Fig. 9*b*, $n = 7$-9, unpaired *t* test, WT: 34, KO: 46, $p = 0.064$, $\eta^2 = 0.157$), and a significant increase in total distance traveled for $P2Y_6R$ KO mice compared with WT mice (Fig. 9*c*, $n = 7$-9, unpaired *t* test, WT: 675, KO: 901, $p = 0.027$, $\eta^2 = 0.239$), suggesting mildly increased motility of $P2Y_6R$ KO mice. Both WT ($n = 9$, one-sample *t* test to 50%, WT: 72, $p = 0.0003$, $\eta^2 = 0.819$) and $P2Y_6R$ KO ($n = 7$, one-sample *t* test to 50%, KO: 60, $p = 0.010$, $\eta^2 = 0.691$) mice conducted spontaneous alterations in the Y-maze, meaning that both groups of mice had short-term spatial memory. However, there was a significant decrease in spontaneous alterations for $P2Y_6R$ KO mice compared with WT mice, reduced from 72% in WT mice to 60% in $P2Y_6R$ KO mice, where 50% indicates random arm entry and zero memory (Fig. 9*d*, $n = 7$-9, unpaired *t* test, WT: 72, KO: 60, $p = 0.013$, $\eta^2 = 0.304$). These data indicate that $P2Y_6R$ KO mice have impaired short-term spatial memory.

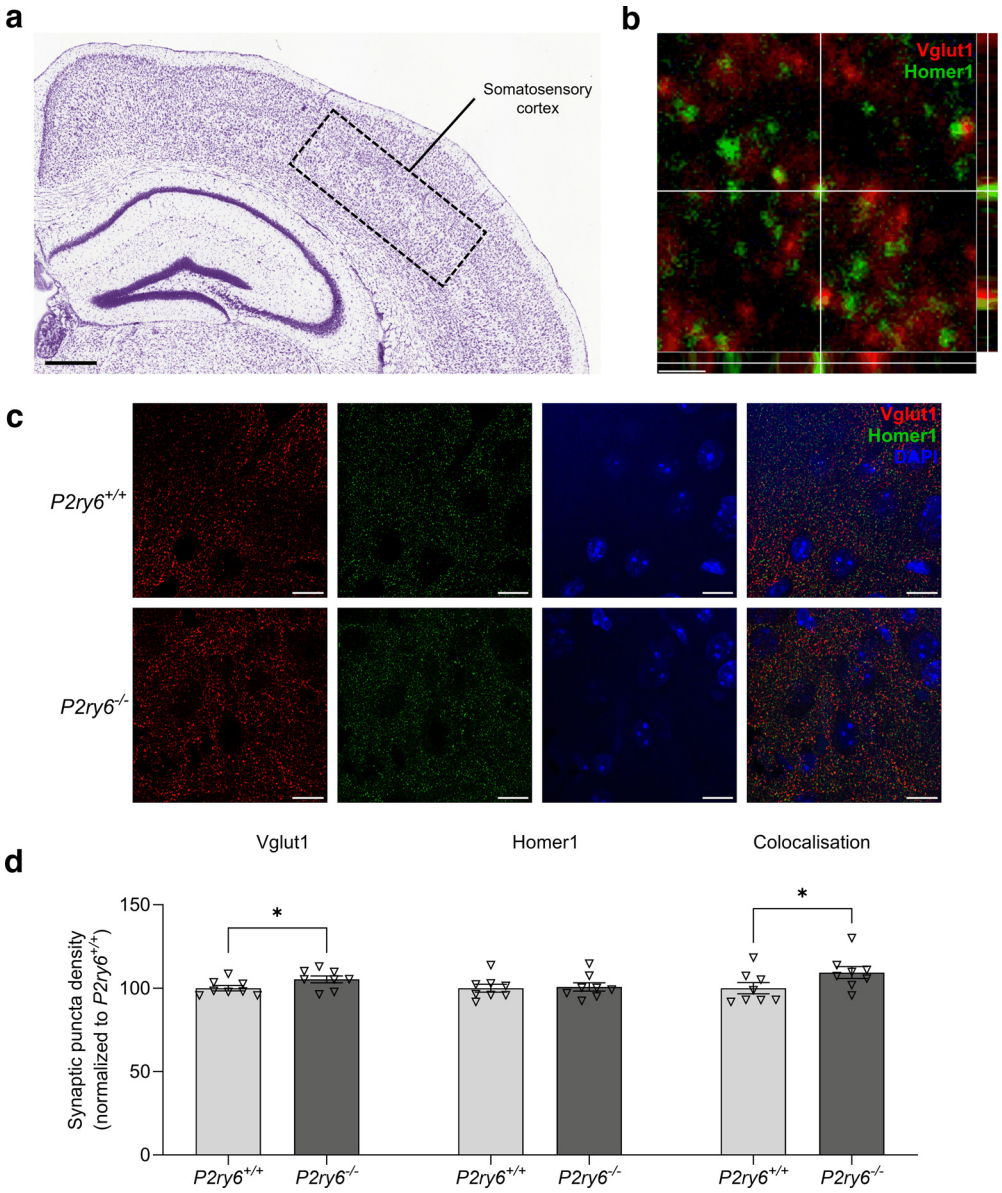

Figure 4. $P2Y_6R$ deficiency results in increased synaptic density in the somatosensory cortex. ***a***, Nissl stain from the Allen Mouse Brain Atlas and Allen Reference Atlas–Mouse Brain of a coronal section of the mouse brain, with the somatosensory cortex labeled. Available from mouse.brain-map.org/static/atlas. ***b***, Colocalization of Vglut1 and Homer1 puncta. Scale bar, 0.5 μm. ***c***, Representative confocal microscopy images of P30 WT and $P2Y_6R$ KO mice stained for Vglut1 (red represents presynaptic marker), Homer1 (green represents postsynaptic marker), and with DAPI (blue represents nuclear stain) in the somatosensory cortex. Scale bar, 5 μm. ***d***, Vglut1 puncta density, Homer1 puncta density, and synaptic density of the somatosensory cortex ($n = 8$, 3 equidistant planes 300 μm apart per mouse). Synaptic density determined as colocalized Vglut1 and Homer1 puncta (<200 nm). Raw values for synaptic puncta density across brain regions are available in Extended Data Figure 4-1. Synaptic internalization by microglia negatively correlates with synaptic density in the somatosensory cortex, as shown in Extended Data Figure 4-2. Each point represents 1 animal. Error bars indicate ± SEM. *$p < 0.05$ (unpaired *t* tests).

Finally, we tested short-term recognition memory of 9- to 12-month-old mice using the NORT. Mice were habituated in an open field for 2 consecutive days; and on the third day, mice were allowed to explore two identical objects for 10 min. Five minutes after training, one of the objects (familiar) was replaced by a new object (novel), and the relative time spent with the novel and familiar objects was quantified (Fig. 9*e*). During the training session, both WT ($n = 7$, one-sample *t* test to 50%, WT: 50, $p = 0.919$, $\eta^2 = 0.002$) and $P2Y_6R$ KO ($n = 7$, one-sample *t* test to 50%, KO: 52, $p = 0.638$, $\eta^2 = 0.039$) mice had no overall preference for either object (Fig. 9*f*). By contrast, during the test, both WT ($n = 7$, one-sample *t* test to 50%, WT: 72, $p = 0.001$, $\eta^2 = 0.860$) and $P2Y_6R$ KO ($n = 7$, one-sample *t* test to 50%, KO: 62, $p = 0.112$, $\eta^2 = 0.685$) mice spent more time with the novel object, meaning that they had short-term memory of the familiar object. However, $P2Y_6R$ KO mice showed a significantly reduced preference for the novel object compared with WT mice (Fig. 9*g*, $n = 7$, unpaired *t* test, WT: 72, KO: 63, $p = 0.044$, $\eta^2 = 0.222$), indicating that KO mice have impaired short-term recognition memory. Overall, our data indicate that adult $P2Y_6R$ KO mice have reduced memory, consistent with the reduced synaptic pruning during development resulting in long-term deficits in brain function.

Discussion

We had previously found that the $P2Y_6R$ regulates microglial phagocytosis of synapses during aging in mice, by measuring

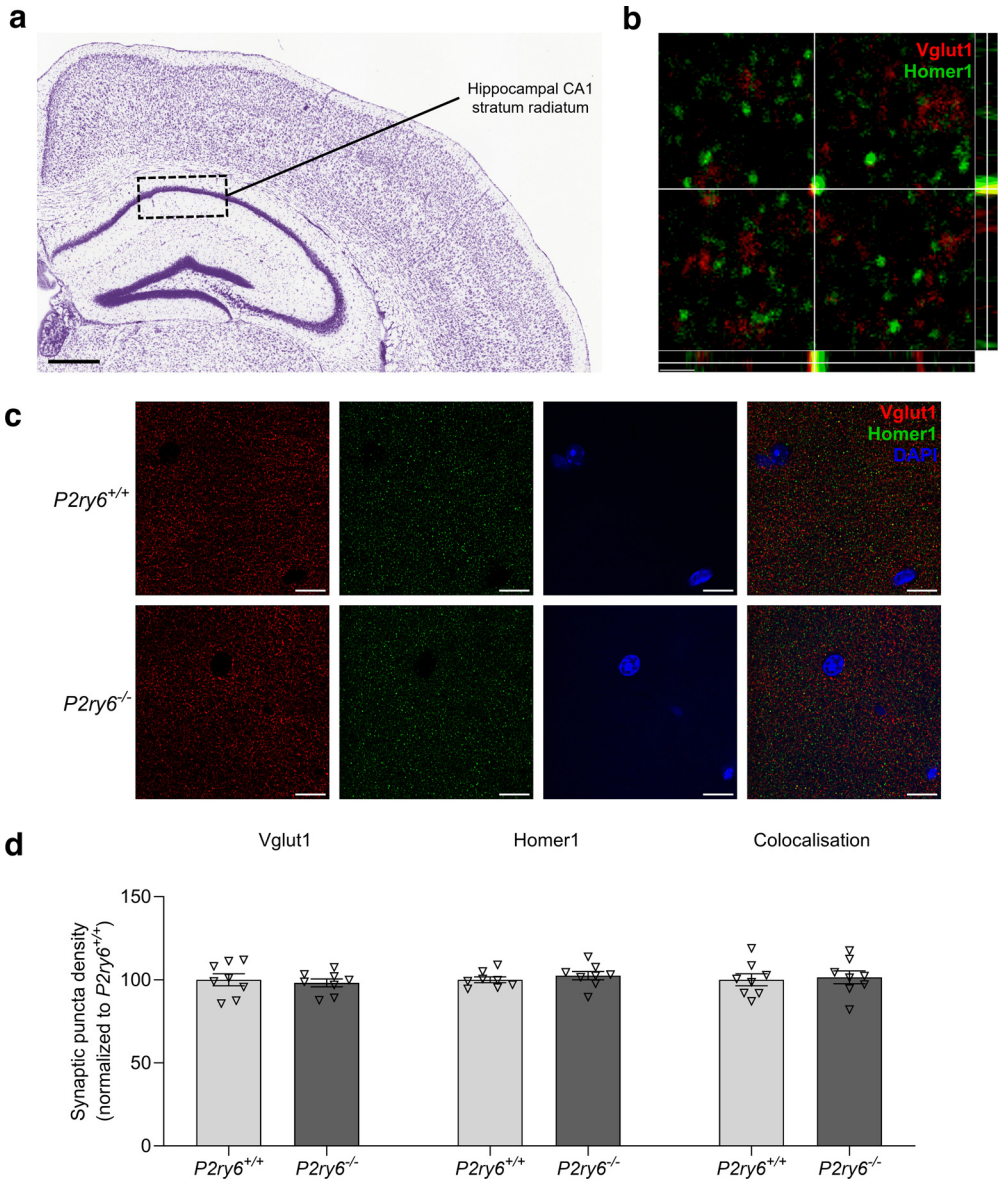

Figure 5. $P2Y_6R$ deficiency does not affect synaptic density in the CA1 hippocampus. ***a***, Nissl stain from the Allen Mouse Brain Atlas and Allen Reference Atlas–Mouse Brain of a coronal section of the mouse brain, with the hippocampal CA1 stratum radiatum labeled. Available from mouse.brain-map.org/static/atlas. ***b***, Colocalization of Vglut1 and Homer1 puncta. Scale bar, 0.5 μm. ***c***, Representative confocal microscopy images of P30 WT and $P2Y_6R$ KO mice stained for Vglut1 (red represents presynaptic marker), Homer1 (green represents postsynaptic marker), and with DAPI (blue represents nuclear stain) in the hippocampal CA1 stratum radiatum. Scale bar, 5 μm. ***d***, Vglut1 puncta density, Homer1 puncta density, and synaptic density of the hippocampal CA1 stratum radiatum ($n = 8$, 3 equidistant planes 300 μm apart per mouse). Synaptic density determined as colocalized Vglut1 and Homer1 puncta (<200 nm). Each point represents 1 animal. Statistical comparisons were made via unpaired *t* tests. Error bars indicate ± SEM.

microglial phagocytosis of isolated synapses, synaptic loss in culture, and synaptic internalization and loss *in vivo* (Dundee et al., 2023). We were therefore interested here in whether $P2Y_6R$ regulates microglial phagocytosis of synapses during development in mice, and if so, whether this affects adult brain function. We found here that $P2Y_6R$ KO mice had greatly reduced synaptic material within microglial lysosomes, and increased synaptic density at P30, consistent with $P2Y_6R$ regulating synaptic pruning. We found that adult $P2Y_6R$ KO mice had impaired long- and short-term memory, consistent with reduced synaptic pruning causing memory dysfunction. Thus, it appears that $P2Y_6R$ mediates synaptic pruning via regulating microglial phagocytosis of synapses during development; and if this does not occur, adult brain dysfunction results. However, there are a number of uncertainties and limitations of our study that are outlined below.

We measured microglial phagocytosis of synapses as the internalization of the presynaptic marker Vglut1 into the CD68-stained lysosomes of Iba1-stained microglia in fixed sections of the somatosensory cortex of WT and $P2Y_6R$ KO mice at P30. We found a large reduction in Vglut1 within microglial lysosomes in the KO mice, consistent with reduced phagocytosis. This is consistent with previous research identifying a role for microglial phagocytosis in developmental synaptic pruning (Tremblay et al., 2010; Paolicelli et al., 2011). However, we did not visualize/image phagocytosis over time, and it is conceivable that the reduced Vglut1 within microglial lysosomes in the KO mice was because of increased digestion of the synaptic material within the KO lysosomes. To directly test this possibility, in our previous publication, we fed isolated synapses (synaptosomes) to immortalized microglia and measured the

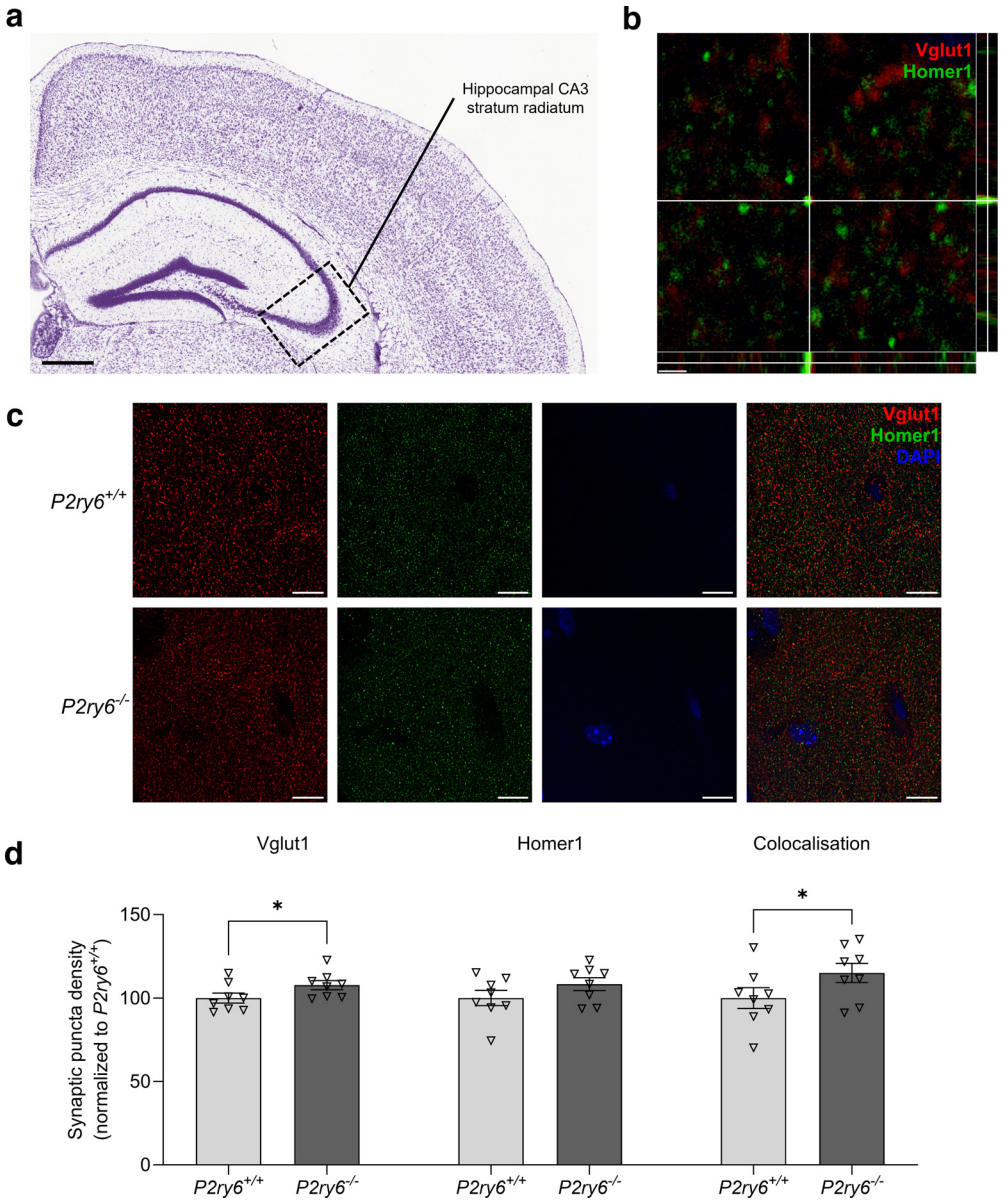

Figure 6. $P2Y_6R$ deficiency results in increased synaptic density in the CA3 hippocampus. ***a***, Nissl stain from the Allen Mouse Brain Atlas and Allen Reference Atlas–Mouse Brain of a coronal section of the mouse brain, with the hippocampal CA3 stratum radiatum labeled. Available from mouse.brain-map.org/static/atlas. ***b***, Colocalization of Vglut1 and Homer1 puncta. Scale bar, 0.5 μm. ***c***, Representative confocal microscopy images of P30 WT and $P2Y_6R$ KO mice stained for Vglut1 (red represents presynaptic marker), Homer1 (green represents postsynaptic marker), and with DAPI (blue represents nuclear stain) in the hippocampal CA3 stratum radiatum. Scale bar, 5 μm. ***d***, Vglut1 puncta density, Homer1 puncta density, and synaptic density of the hippocampal CA3 stratum radiatum ($n = 8$, 3 equidistant planes 300 μm apart per mouse). Synaptic density determined as colocalized Vglut1 and Homer1 puncta (<200 nm). Each point represents 1 animal. Error bars indicate ± SEM. *$p < 0.05$ (unpaired *t* tests).

rate of Vglut1 degradation with and without the $P2Y_6R$ inhibitor MRS2578 and found no difference in Vglut1 degradation rate (Dundee et al., 2023). Moreover, we showed that microglia isolated from $P2Y_6R$ KO mice had a reduced rate of microglial phagocytosis of the isolated synapses (Dundee et al., 2023). Thus, the reduced Vglut1 within microglial lysosomes in the KO mice found here is most likely because of reduced microglial phagocytosis of synapses. However, additional experiments should be conducted on $P2Y_6R$ KO microglial lysosomes to test for possible functional deficits, such as lysosomal acidity and enzyme composition.

We chose a presynaptic marker (Vglut1), rather than a postsynaptic marker, as there is clearer evidence for microglial phagocytosis of presynaptic markers during development (Weinhard et al., 2018; Mordelt and de Witte, 2023). However, it would be interesting to know whether $P2Y_6R$ also affects microglial phagocytosis of postsynaptic elements, such as dendritic spines, or the microglial phagocytosis of inhibitory synapses. We chose to examine synapse phagocytosis and density at P30 because synaptic pruning has been reported to still be actively occurring in somatosensory cortex of mice at this time point (Cong et al., 2020). However, it would be useful to know whether $P2Y_6R$ affects microglial phagocytosis at other developmental time points, including adults. We chose somatosensory cortex because there is evidence for a role in working memory and we have previously identified $P2Y_6R$-dependent phagocytosis occurring in this region (Long and Zhang, 2021; Dundee et al., 2023), but it would be informative to look at other areas of the brain.

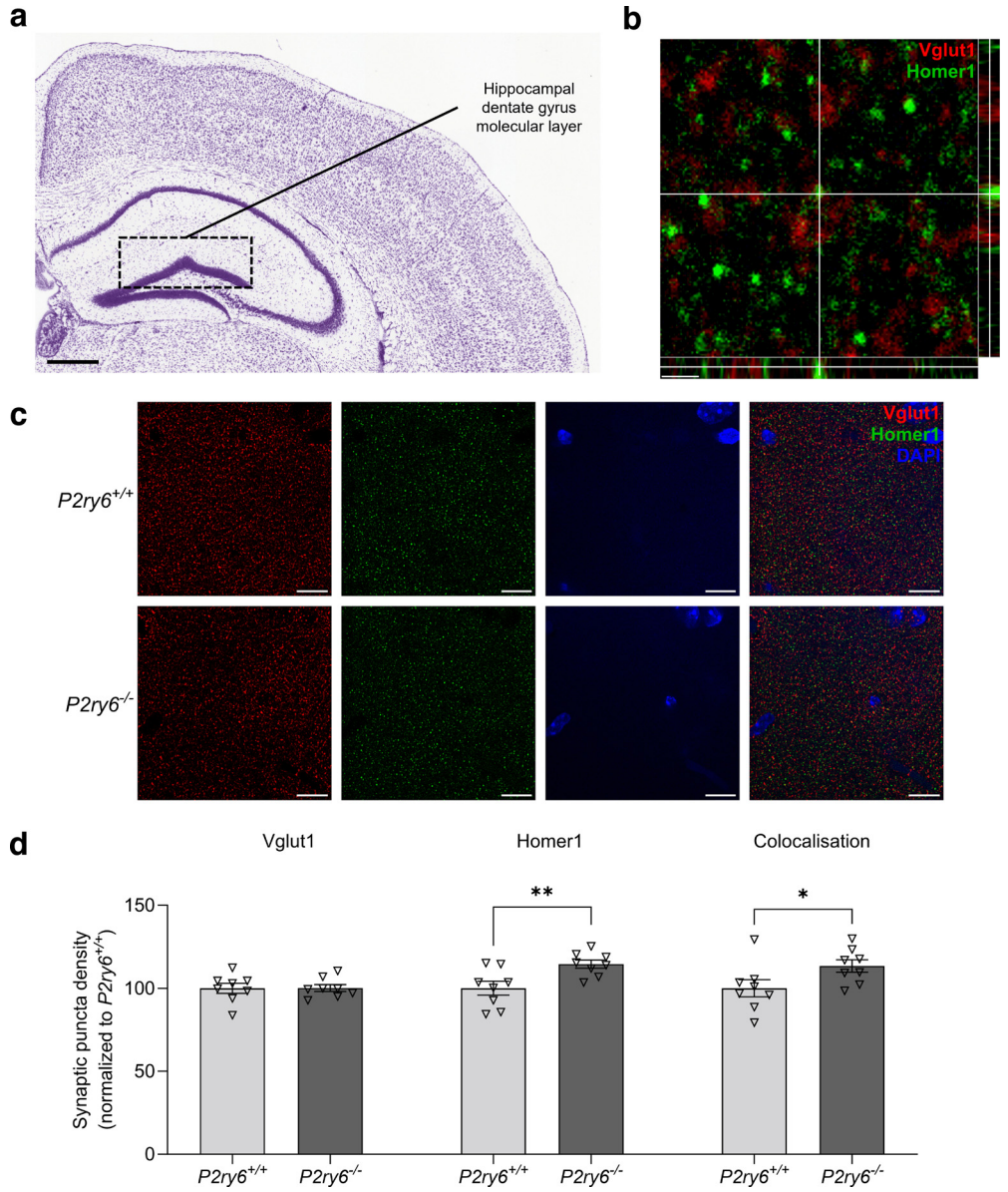

Figure 7. $P2Y_6R$ deficiency results in increased synaptic density in the dentate gyrus. ***a***, Nissl stain from the Allen Mouse Brain Atlas and Allen Reference Atlas–Mouse Brain of a coronal section of the mouse brain, with the hippocampal dentate gyrus molecular layer labeled. Available from mouse.brain-map.org/static/atlas. ***b***, Colocalization of Vglut1 and Homer1 puncta. Scale bar, 0.5 μm. ***c***, Representative confocal microscopy images of P30 WT and $P2Y_6R$ KO mice stained for Vglut1 (red represents presynaptic marker), Homer1 (green represents postsynaptic marker), and with DAPI (blue represents nuclear stain) in the hippocampal dentate gyrus molecular layer. Scale bar, 5 μm. ***d***, Vglut1 puncta density, Homer1 puncta density, and synaptic density of the hippocampal dentate gyrus molecular layer ($n = 8$, 3 equidistant planes 300 μm apart per mouse). Synaptic density determined as colocalized Vglut1 and Homer1 puncta (<200 nm). Each point represents 1 animal. Error bars indicate ± SEM. *$p < 0.05$ (unpaired *t* tests).

We measured synapse density as the density of Vglut1-staining puncta, Homer1-staining puncta, and their colocalization (<200 nm) within the *Z* stack of 25-μm-thick brain sections using confocal microscopy. Thick sections have limitations with confocal microscopy, especially in relation to the *z* plane (Avila and Henstridge, 2022), so ideally our data should be verified using array tomography of ultrathin sections. Vglut1 and Homer1 puncta density is high in the hippocampal stratum radiatum and molecular layer, as well as the somatosensory cortex, because of the high density of glutamatergic synapses. However, in the hippocampal stratum lacunosum-moleculare, Vglut1 puncta density is substantially lower compared with Vglut2 puncta density as Vglut2 is found primarily on output neurons in the hippocampus (Wozny et al., 2018). It may be beneficial to use excitatory synaptic markers that are less region-specific for future studies, such as synaptophysin and PSD-95, as well as investigate inhibitory synapses. We analyzed synapses at a single time point (P30) in mouse development, and it would be useful to analyze other time points to understand how $P2Y_6R$ affects changes in synapses during development.

We found a subtle increase in synaptic density in $P2Y_6R$ KO mice, consistent with reduced microglial phagocytosis of synapses. However, this finding is also consistent with increased synaptogenesis or reduced retraction of synapses in the KO mice. On the other hand, as there is clear evidence from us and others that $P2Y_6R$ mediates microglial phagocytosis (Koizumi et al., 2007; Puigdellívol et al., 2021; Dundee et al., 2023), but there is no evidence that $P2Y_6R$ affects synaptogenesis or synapse retraction, the most parsimonious explanation of our finding of

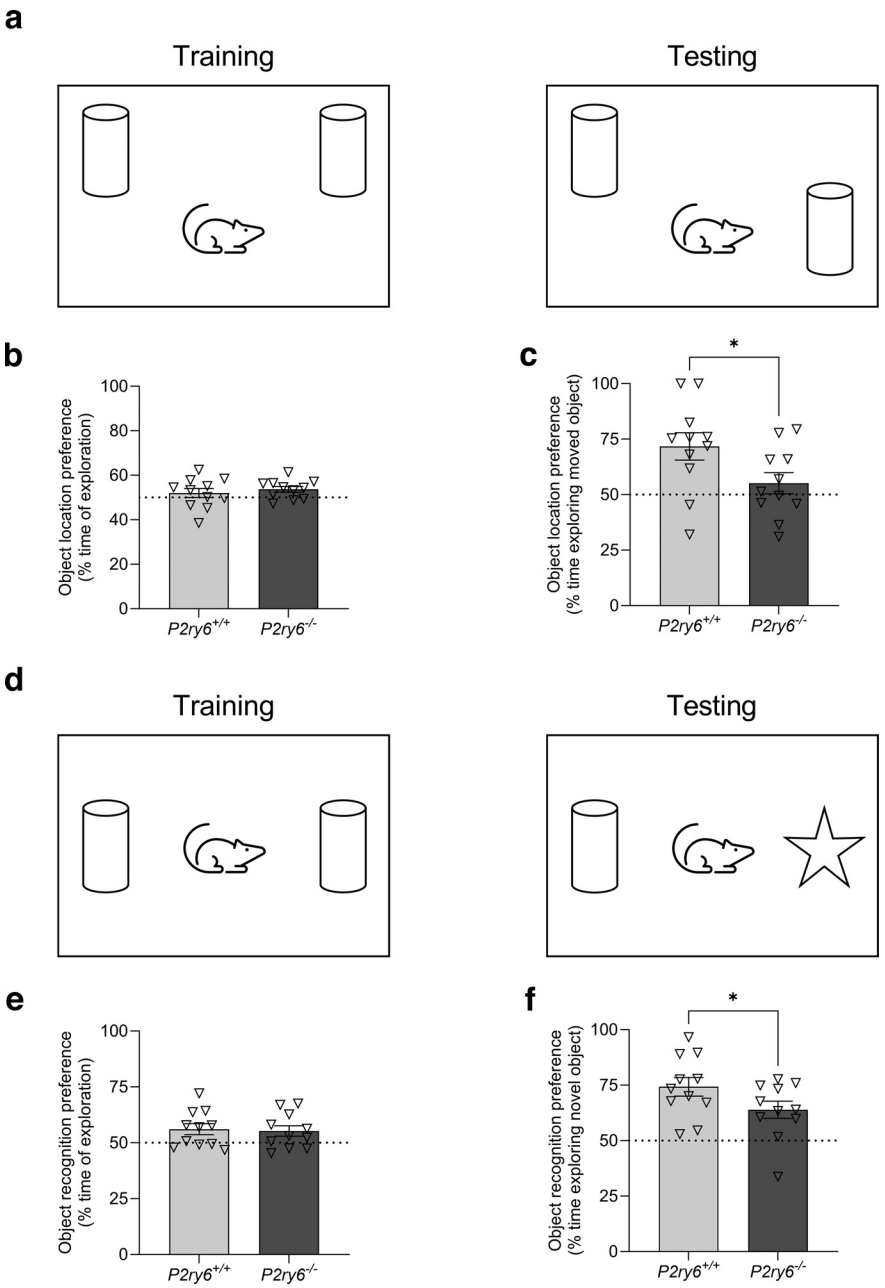

Figure 8. $P2Y_6R$ deficiency results in long-term memory loss. ***a***, Schematic representation of the training and testing sessions in the NORT. ***b***, Object preference of each animal as percentage of time spent exploring two identical objects ($n = 11$). ***c***, Object preference of each animal as percentage of time spent exploring the novel object 24 h after training ($n = 11$). ***d***, Schematic representation of the training and testing sessions in the OLRT. ***e***, Object preference of each animal as percentage of time spent exploring two identical objects ($n = 11$). ***f***, Object preference of each animal as percentage of time spent exploring the novel object 24 h after training ($n = 11$). ***b***, ***c***, Data were reanalyzed from Dundee et al. (2023). Each point represents 1 animal. Dashed lines indicate a 50% chance level. Error bars indicate ± SEM. *$p < 0.05$ (unpaired *t* tests).

increased synaptic density in the $P2Y_6R$ KOs is reduced microglial phagocytosis of synapses, for which we have independent evidence. However, it would be useful to test the effect of $P2Y_6R$ KO on other potential regulators of synaptic density. It would also be interesting to look at the effect of $P2Y_6R$ KO on the density of particular synaptic types, such as inhibitory synapses.

We found that adult $P2Y_6R$ KO mice had reduced short- and long-term memory, consistent with reduced synaptic pruning during development causing memory dysfunction. However, the memory defects of adult mice could result from reduced microglial phagocytosis of synapses in the adult mice, because such phagocytosis has been found to contribute to learning and memory in the adult brain (Miyanishi et al., 2021). This might be clarified by testing memory at earlier ages, or using conditional KO of $P2Y_6R$. However, if learning and memory are regulated by $P2Y_6R$-dependent microglial phagocytosis of synapses, it may be difficult to disentangle a developmental effect from an adult effect. We have attributed the reduced memory of $P2Y_6R$ KO mice to reduced synaptic pruning during development; however, it cannot be ruled out that the memory deficits result from other effects of $P2Y_6R$ yet to be discovered. We have previously reported that $P2Y_6R$ KO mice have improved memory when 17 months old relative to WT mice, which have strongly degraded memory at

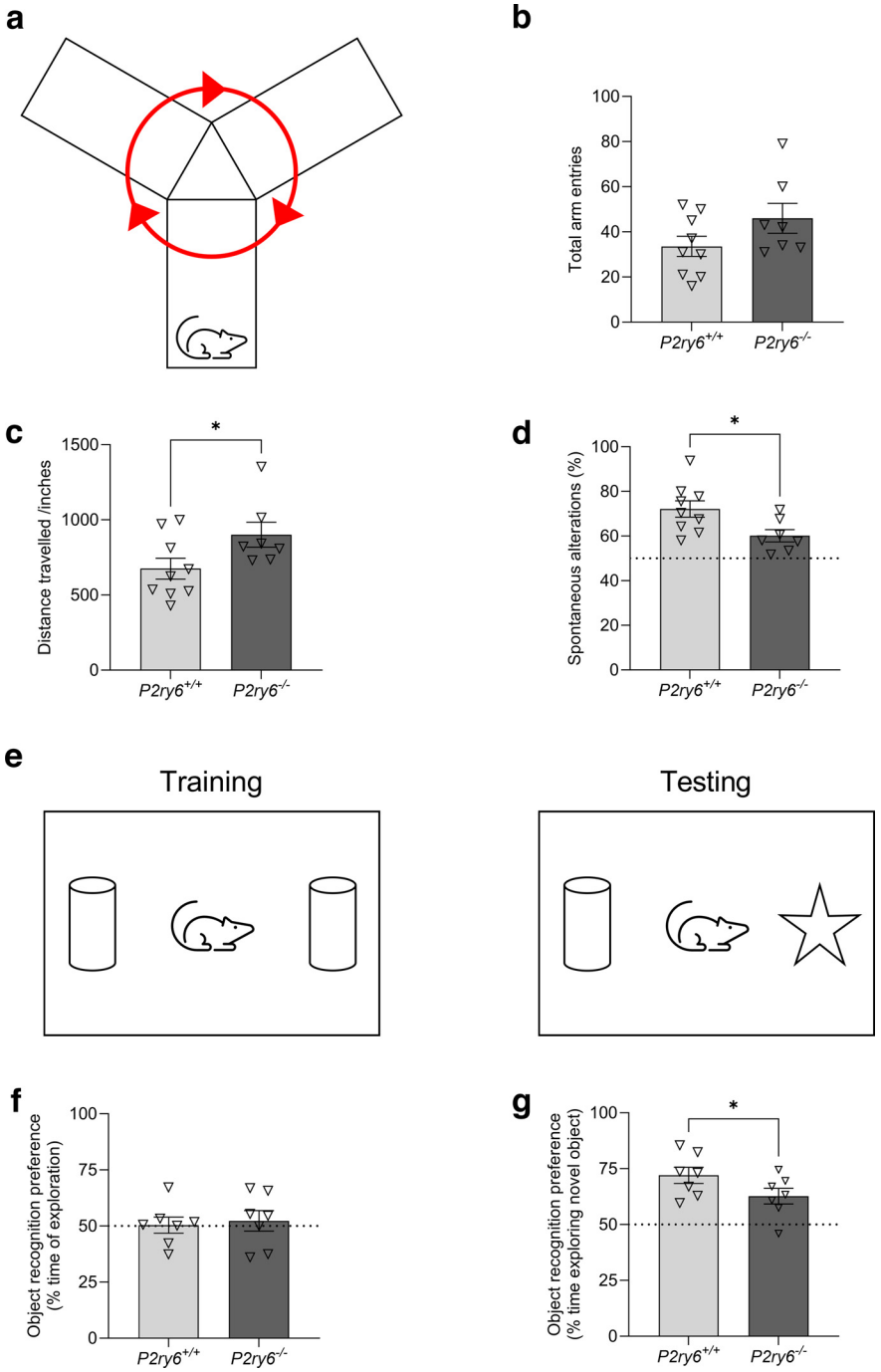

Figure 9. $P2Y_6R$ deficiency results in short-term memory loss. ***a***, Schematic representation of spontaneous alterations in the Y-maze. ***b***, Total number of arm entries by each animal in the Y-maze ($n = 7$-9). ***c***, Distance traveled (inches) by each animal in the Y-maze ($n = 7$–9). ***d***, Spontaneous alterations by each animal in the Y-maze ($n = 7$–9). ***e***, Schematic representation of the training and testing sessions in the NORT. ***f***, Object preference of each animal as percentage of time spent exploring two identical objects ($n = 7$). ***g***, Object preference of each animal as percentage of time spent exploring the novel object 24 h after training ($n = 7$). ***f***, ***g***, Data were reanalyzed from Puigdellívol et al. (2021). Each point represents 1 animal. Dashed lines indicate a 50% chance level. Error bars indicate ± SEM. *$p < 0.05$ (unpaired *t* tests).

this age (Dundee et al., 2023). We attributed this protection to $P2Y_6R$ mediating the excessive microglial phagocytosis of synapses occurring at this age (Dundee et al., 2023). Thus, $P2Y_6R$-regulated phagocytosis of synapses may potentially protect memory in the young and degrade memory in the old.

Disruption of synaptic pruning can lead to behavioral deficits in mice, reminiscent of neurodevelopmental disorders, such as autism and schizophrenia, suggesting that these disorders result from disrupted microglial phagocytosis of synapses (Faust et al., 2021; Mordelt and de Witte, 2023). It would therefore be interesting to test young $P2Y_6R$ KO mice for behaviors, such as socialization, related to neurodevelopmental disorders. However, socialization deficits have been linked to specific neuronal-microglial signaling, such as via fractalkine (Corona et al., 2010), rather than microglia per se (Mordelt and de Witte, 2023). It is unclear what behavioral effects may result from loss of UDP-$P2Y_6R$ signaling, but it would be interesting to investigate further.

$P2Y_6R$ is a receptor on microglia for extracellular UDP, and extracellular UDP acutely induces microglial phagocytosis (Koizumi et al., 2007). Kainate-stressed neurons have been shown to release UTP that is converted to UDP in the mouse brain (Koizumi et al., 2007), and amyloid β-stressed neurons have also been shown to release UDP that activates $P2Y_6R$ (Puigdellívol et al., 2021). UTP is known to be released from stressed or apoptotic cells via pannexin or connexin channels (Elliott et al., 2009; Lazarowski, 2012). UDP activation of $P2Y_6R$ induces formation of the phagocytic cup in microglia, which is a late stage in the engulfment process, normally preceded by recognition of other phagocytic signals on the target. Thus, UDP-$P2Y_6R$ signaling may potentially combine with other signals to recognize synapses that should be engulfed (Cockram et al., 2021). It would be useful to test whether and in what conditions synapses release UDP (although this is currently difficult to do), and how UDP might combine with other signals on the synapse to regulate microglial phagocytosis of synapses.

References

Avila AS, Henstridge CM (2022) Array tomography: 15 years of synaptic analysis. Neuronal Signal 6:NS20220013.

Cockram TO, Dundee JM, Popescu AS, Brown GC (2021) The phagocytic code regulating phagocytosis of mammalian cells. Front Immunol 12:629979.

Cong Q, Soteros BM, Wollet M, Kim JH, Sia GM (2020) The endogenous neuronal complement inhibitor SRPX2 protects against complement-mediated synapse elimination during development. Nat Neurosci 23:1067–1078.

Corona AW, Huang Y, O'Connor JC, Dantzer R, Kelley KW, Popovich PG, Godbout JP (2010) Fractalkine receptor (CX3CR1) deficiency sensitizes mice to the behavioral changes induced by lipopolysaccharide. J Neuroinflammation 7:93.

Davis RA, Lii K-S, Politis DN (1956) Remarks on some nonparametric estimates of a density function. In Selected Works of Murray Rosenblatt, pp 832–837. Springer.

Dundee JM, Puigdellívol M, Butler R, Cockram TO, Brown GC (2023) P2Y6 receptor-dependent microglial phagocytosis of synapses mediates synaptic and memory loss in aging. Aging Cell 22:1–14.

Elliott MR, Chekeni FB, Trampont PC, Lazarowski ER, Kadl A, Walk SF, Park D, Woodson RI, Ostankovich M, Sharma P, Lysiak JJ, Harden TK, Leitinger N, Ravichandran KS (2009) Nucleotides released by apoptotic cells act as a find-me signal to promote phagocytic clearance. Nature 461:282–286.

Ennaceur A, Delacour J (1988) A new one-trial test for neurobiological studies of memory in rats: 1. Behavioral data. Behav Brain Res 31:47–59.

Faust TE, Gunner G, Schafer DP (2021) Mechanisms governing activity-dependent synaptic pruning in the developing mammalian CNS. Nat Rev Neurosci 22:657–673.

Gabandé-Rodríguez E, Keane L, Capasso M (2020) Microglial phagocytosis in aging and Alzheimer's disease. J Neurosci Res 98:284–298.

Hainmueller T, Bartos M (2020) Dentate gyrus circuits for encoding, retrieval and discrimination of episodic memories. Nat Rev Neurosci 21:153–168.

Hong S, Beja-Glasser VF, Nfonoyim BM, Frouin A, Li S, Ramakrishnan S, Merry KM, Shi Q, Rosenthal A, Barres BA, Lemere CA, Selkoe DJ, Stevens B (2016a) Complement and microglia mediate early synapse loss in Alzheimer mouse models. Science 352:712–716.

Hong S, Dissing-Olesen L, Stevens B (2016b) New insights on the role of microglia in synaptic pruning in health and disease. Curr Opin Neurobiol 36:128–134.

Koizumi S, Shigemoto-Mogami Y, Nasu-Tada K, Shinozaki Y, Ohsawa K, Tsuda M, Joshi BV, Jacobson KA, Kohsaka S, Inoue K (2007) UDP acting at P2Y6 receptors is a mediator of microglial phagocytosis. Nature 446:1091–1095.

Kraeuter AK, Guest PC, Sarnyai Z (2019) The Y-maze for assessment of spatial working and reference memory in mice. Methods Mol Biol 1916:105–111.

Lazarowski ER (2012) Vesicular and conductive mechanisms of nucleotide release. Purinergic Signal 8:359–373.

Long X, Zhang SJ (2021) A novel somatosensory spatial navigation system outside the hippocampal formation. Cell Res 31:649–663.

Milde S, van Tartwijk FW, Vilalta A, Hornik TC, Dundee JM, Puigdellívol M, Brown GC (2021) Inflammatory neuronal loss in the substantia nigra induced by systemic lipopolysaccharide is prevented by knockout of the P2Y6 receptor in mice. J Neuroinflammation 18:225–229.

Miyanishi K, Sato A, Kihara N, Utsunomiya R, Tanaka J (2021) Synaptic elimination by microglia and disturbed higher brain functions. Neurochem Int 142:104901.

Mordelt A, de Witte LD (2023) Microglia-mediated synaptic pruning as a key deficit in neurodevelopmental disorders: hype or hope? Curr Opin Neurobiol 79:102674.

Moreno Manrique JF, Voit PR, Windsor KE, Karla AR, Rodriguez SR, Beaudoin GMJ (2021) SynapseJ: an automated, synapse identification macro for ImageJ. Front Neural Circuits 15:731333.

Murai T, Okuda S, Tanaka T, Ohta H (2007) Characteristics of object location memory in mice: behavioral and pharmacological studies. Physiol Behav 90:116–124.

Neher JJ, Neniskyte U, Hornik T, Brown GC (2014) Inhibition of UDP/P2Y6 purinergic signaling prevents phagocytosis of viable neurons by activated microglia in vitro and in vivo. Glia 62:1463–1475.

Otsu N, Smith PL, Reid DB, Environment C, Palo L, Alto P, Smith PL (1979) A threshold selection method from gray-level histograms. IEEE Trans Syst Man Cybern 9:62–66.

Paolicelli RC, Bolasco G, Pagani F, Maggi L, Scianni M, Panzanelli P, Giustetto M, Ferreira TA, Guiducci E, Dumas L, Ragozzino D, Gross CT (2011) Synaptic pruning by microglia is necessary for normal brain development. Science 333:1456–1458.

Prieur E, Jadavji N (2019) Assessing spatial working memory using the spontaneous alternation Y-maze test in aged male mice. Bio-Protocol 9:1–10.

Puigdellívol M, Milde S, Vilalta A, Cockram TO, Allendorf DH, Lee JY, Dundee JM, Pampuščenko K, Borutaite V, Nuthall HN, Brelstaff JH, Spillantini MG, Brown GC (2021) The microglial P2Y6 receptor mediates neuronal loss and memory deficits in neurodegeneration. Cell Rep 37:110148.

Rebola N, Carta M, Mulle C (2017) Operation and plasticity of hippocampal CA3 circuits: implications for memory encoding. Nat Rev Neurosci 18:208–220.

Schafer DP, Lehrman EK, Kautzman AG, Koyama R, Mardinly AR, Yamasaki R, Ransohoff RM, Greenberg ME, Barres BA, Stevens B (2012) Microglia sculpt postnatal neural circuits in an activity and complement-dependent manner. Neuron 74:691–705.

Schafer DP, Lehrman EK, Heller CT, Stevens B (2014) An engulfment assay: a protocol to assess interactions between CNS phagocytes and neurons. J Vis Exp 88:e51482.

Schindelin J, Arganda-Carreras I, Frise E, Kaynig V, Longair M, Pietzsch T, Preibisch S, Rueden C, Saalfeld S, Schmid B, Tinevez JY, White DJ, Hartenstein V, Eliceiri K, Tomancak P, Cardona A (2012) Fiji: an open-source platform for biological-image analysis. Nat Methods 9:676–682.

Sierra A, Abiega O, Shahraz A, Neumann H (2013) Janus-faced microglia: beneficial and detrimental consequences of microglial phagocytosis. Front Cell Neurosci 7:6–22.

Stevens B, Allen NJ, Vazquez LE, Howell GR, Christopherson KS, Nouri N, Micheva KD, Mehalow AK, Huberman AD, Stafford B, Sher A, Litke AM, Lambris JD, Smith SJ, John SW, Barres BA (2007) The classical complement cascade mediates CNS synapse elimination. Cell 131:1164–1178.

Tang Y, Nyengaard JR, De Groot DM, Gundersen HJ (2001) Total regional and global number of synapses in the human brain neocortex. Synapse 41:258–273.

Tay TL, Béchade C, D'Andrea I, St-Pierre MK, Henry MS, Roumier A, Tremblay ME (2018) Microglia gone rogue: impacts on psychiatric disorders across the lifespan. Front Mol Neurosci 10:421–426.

Tremblay M, Lowery RL, Majewska AK (2010) Microglial interactions with synapses are modulated by visual experience. PLoS Biol 8:e1000527.

Vogel-Ciernia A, Wood MA (2014) Examining object location and object recognition memory in mice. Curr Protoc Neurosci 69:8.31.1–8.31.17.

Wang YY, Deng YS, Dai SK, Mi TW, Li RY, Liu PP, Liu C, He BD, He XC, Du HZ, Yang HC, Tang Y, Liu CM, Teng ZQ (2022) Loss of microglial EED impairs synapse density, learning, and memory. Mol Psychiatry 27:2999–3009.

Weinhard L, Di Bartolomei G, Bolasco G, Machado P, Schieber NL, Neniskyte U, Exiga M, Vadisiute A, Raggioli A, Schertel A, Schwab Y, Gross CT (2018) Microglia remodel synapses by presynaptic trogocytosis and spine head filopodia induction. Nat Commun 9:1228.

Wolf SA, Boddeke HW, Kettenmann H (2017) Microglia in physiology and disease. Annu Rev Physiol 79:619–643.

Wozny C, Beed P, Nitzan N, Pössnecker Y, Rost BR, Schmitz D (2018) VGLUT2 functions as a differential marker for hippocampal output neurons. Front Cell Neurosci 12:337.

Xiao X, Feng YP, Du B, Sun HR, Ding YQ, Qi JG (2017) Antibody incubation at 37°C improves fluorescent immunolabeling in free-floating thick tissue sections. Biotechniques 62:115–122.

York EM, Ledue JM, Bernier LP, Macvicar BA (2018) 3DMorph automatic analysis of microglial morphology in three dimensions from ex vivo and in vivo imaging. eNeuro 5:ENEURO.0266-18.2018.